Electronic Supplementary Material (ESI) for Journal of Materials Chemistry C.

Electronic Supporting Information

Poly(dimethylsiloxane) functionalized with complementary organic and inorganic emitters for the design of white emissive waveguides.

Soumaya Khlifi,[a] John Bigeon,[a] Maria Amela-Cortes,[a] Noée Dumait,[a] Huriye Akdas-Kiliç,[a,b] Grégory Taupier,[a] Stéphane Freslon,[a] Stéphane Cordier,[a] Sylvie Derien,[a] Mathieu Achard,[a] Goulc'hen Loas,[a,*] and Yann Molard[a,*]

[a]Univ Rennes, CNRS, INSA, ISCR - UMR 6226, ScanMAT – UMS 2001, Institut FOTON – UMR6082, F-35000 Rennes, France ; yann.molard@univ-rennes1.fr, goulc-hen.loas@univ-rennes1.fr
[b]Yildiz Technical University, Department of Chemistry, 34220 Esenler, Istanbul, Turkey.

Förster radius determination

The following Forster rate equation describes the energy transfer by dipolar interaction:

$$k = \frac{1}{\tau_D}(\frac{R_0}{r})^6, R_0^6 = 8.785 \times 10^{-5}\frac{K^2 \Phi_D J}{n^4}$$

Where τ_D is the donor lifetime in the absence of acceptor, r is the donor-acceptor distance, and R_0 is the Förster distance at which the energy transfer rate is equal to the decay rate. The Förster distance is related to the orientation factor, K^2 between donor and acceptor, and the donor and acceptor spectroscopic properties. K was taken as 2/3 that is appropriate for dynamic random orientation averaging of the donor and acceptor. Φ_D is the quantum yield of the donor in the absence of an acceptor (0.45 for P_{Oxi}). The index of refraction, n, is the index of refraction of PDMS: 1.42. J is the overlap integral between the donor and acceptor that is calculated using the following equation:

$$J = \int_0^{+\infty} F_D\,(\lambda)\varepsilon_A(\lambda)\lambda^4 d\lambda$$

Where F_D is the area-normalized fluorescence spectrum of the donor,[1] ε_A is the molar absorption coefficient of the acceptor. The scaling constant is set such that when ε is in units of $M^{-1}.cm^{-1}$ and wavelength in units of nm, the Förster distance is in units of Å.[2]
The Förster radius was evaluated at 298K.

Supplementary figures

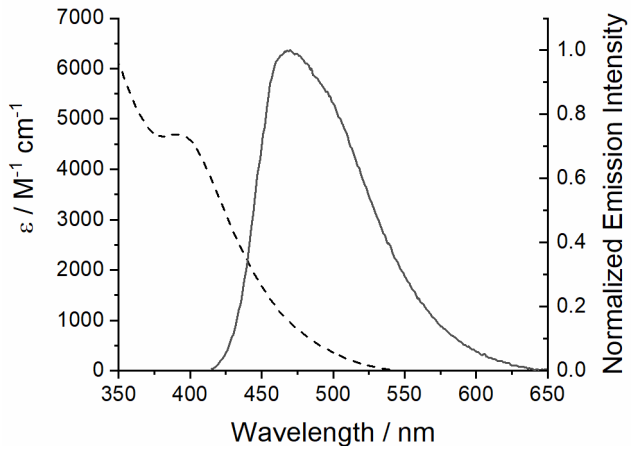

Figure S1. Absorption spectrum (dashed line) of $Cs_2Mo_6I_8(OCOC_2F_5)_6$ in CH_3CN and normalized emission spectrum of P_{oxi} (plain line) used to determine the overlap integral.

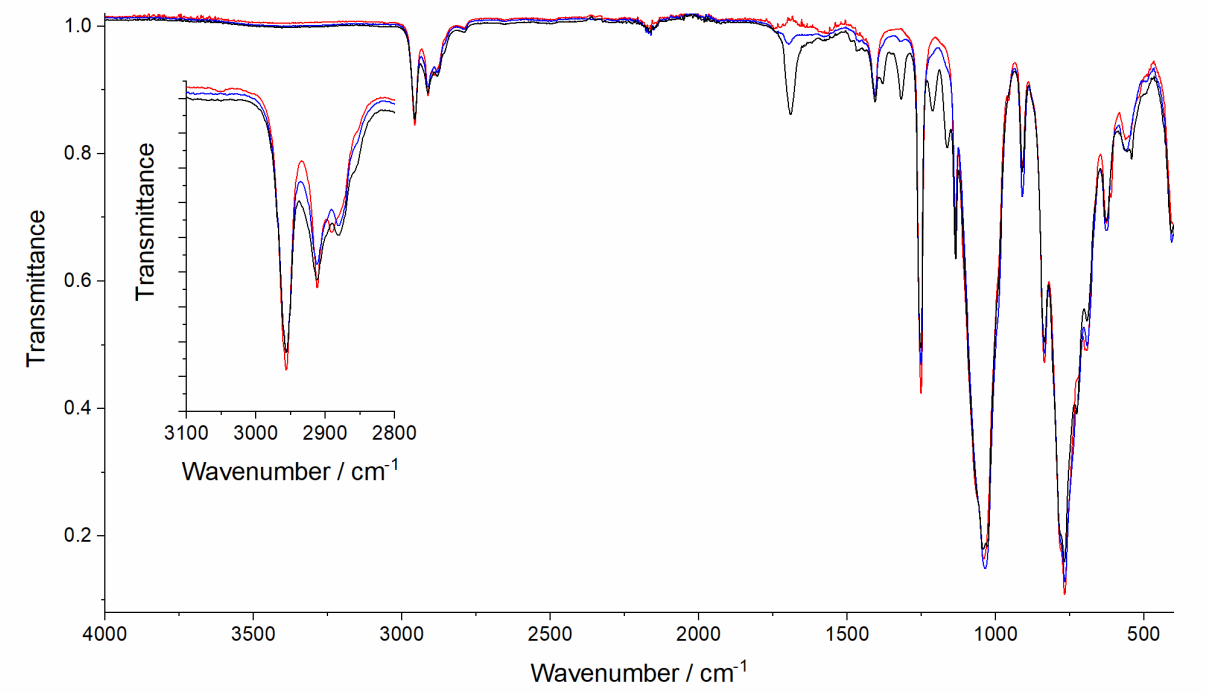

Figure S2. ATR IR spectra of P_{hyb} (black), P_{Mo} (red) and P_{oxi} (blue).

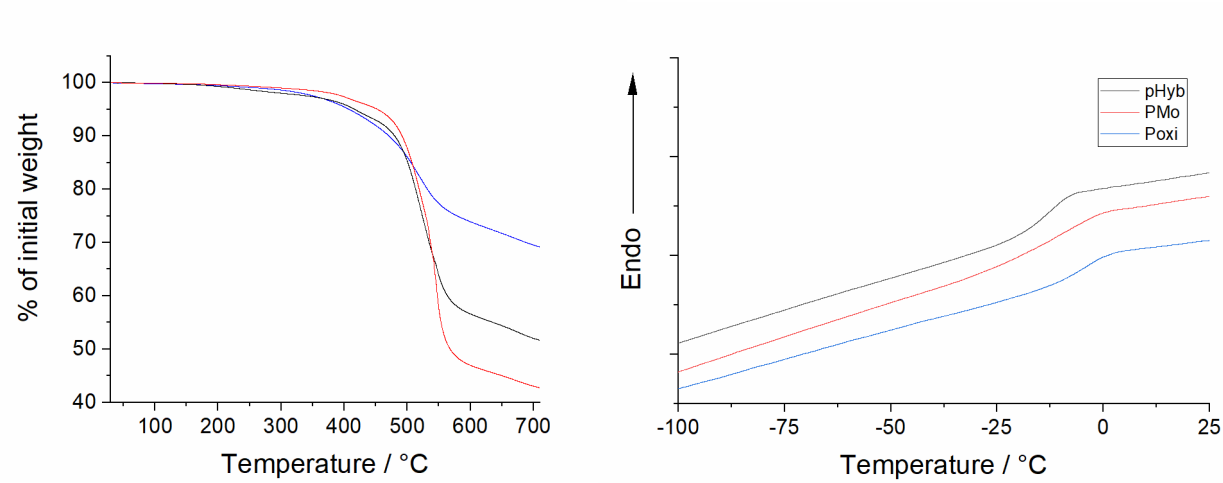

Figure S3. TGA thermograms (left) and DSC thermograms (right) obtained from the second heating cycle for P_{hyb} (black), P_{Mo} (red) and P_{oxi} (blue).

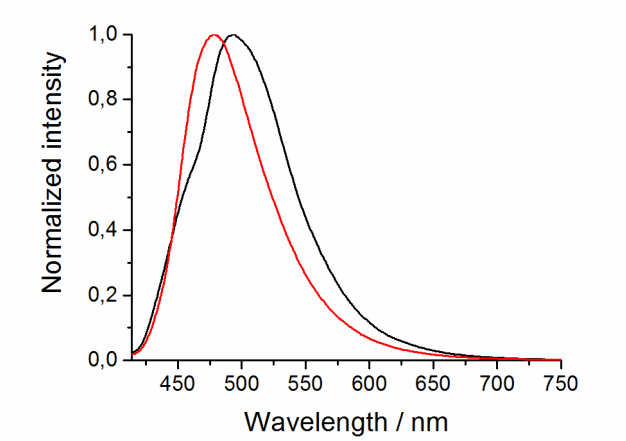

Figure S4. Emission spectra of P_{oxi} under air (red line) and vacuum (black line).

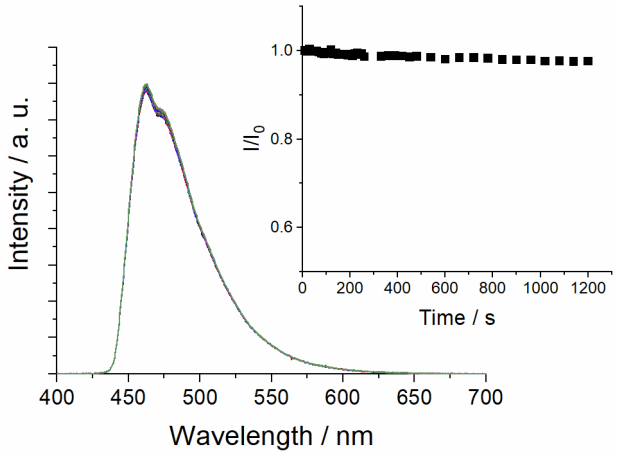

Figure S5. Behavior of P_{oxi} emission under continuous irradiation; inset: intensity at 462 nm *vs* irradiation time.

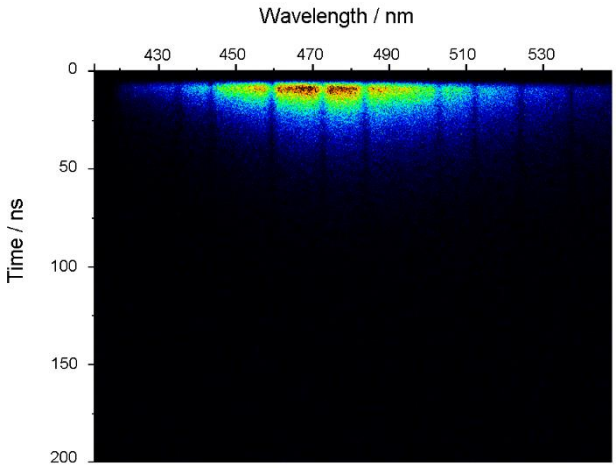

Figure S6. Emission decay map of P_{oxi} fluorescence in air.

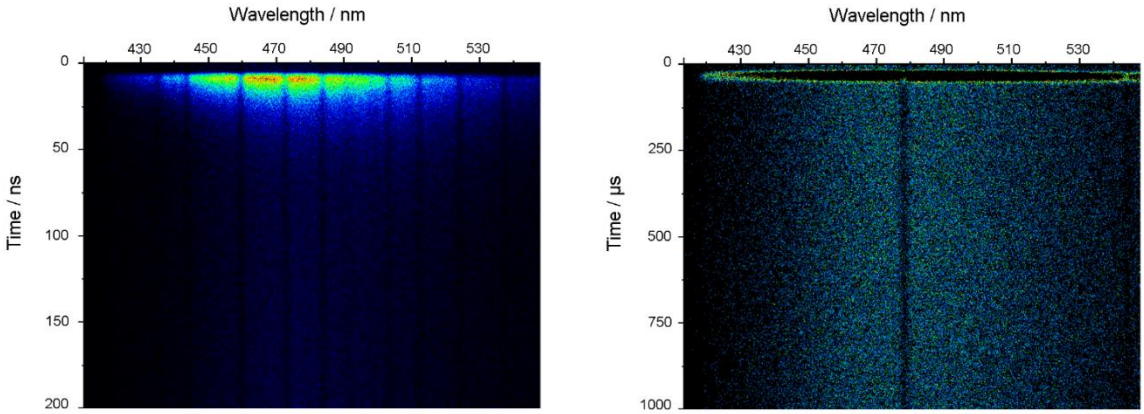

Figure S7. Emission decay map of P_{oxi} in vacuum (left: fluorescence; right detected phosphorescence with the maximum time range of the streak camera).

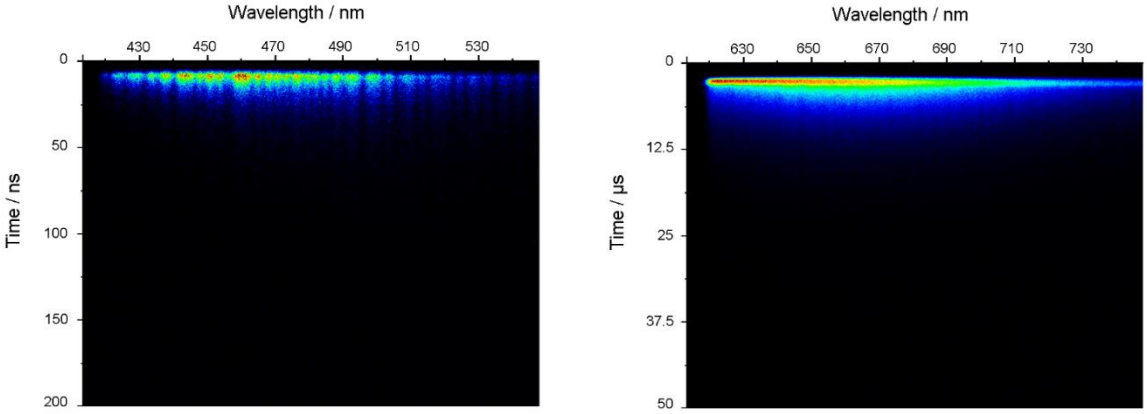

Figure S8. Emission decay map of P_{hyb} in air (left: fluorescence of Oxi; right phosphorescence of Mo_6).

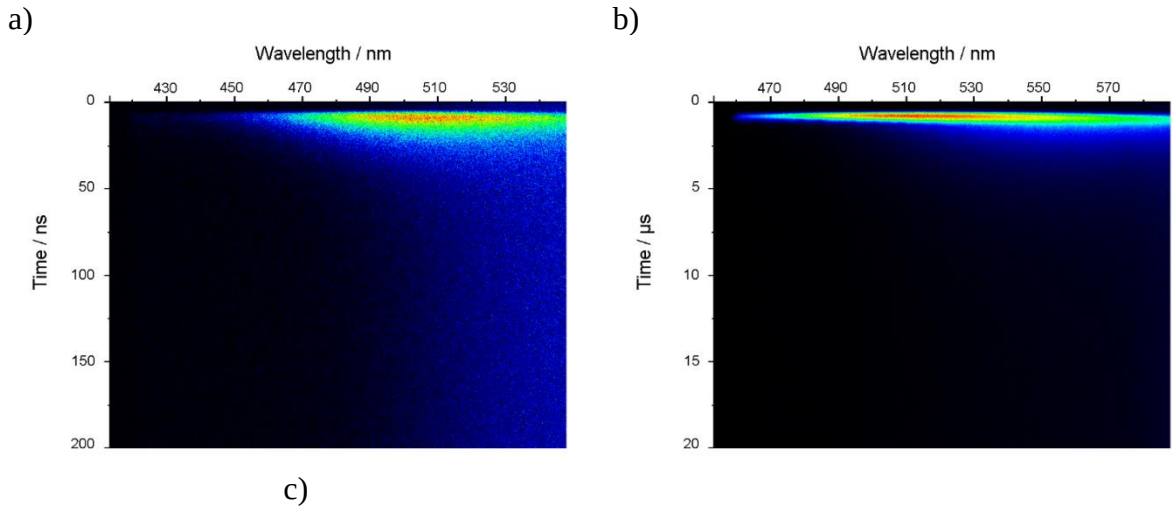

Figure S9. Emission decay map of P_{hyb} in vacuum a) fluorescence of Oxi; the blue halo corresponds to the Oxi phosphorescence that is also detected in b); c) phosphorescence of Mo_6.

Table S1. Fluorescence and phosphorescence average excited state lifetime evolution with temperature for all designed hybrids.

T (K)	**P_{oxi}**		**P_{Mo}**	**P_{hyb}**		
	F (ns)	*P* (ms)	*P* (µs)	*Foxi* (ns)	*Poxi* (ms)	*PMo* (µs)
77	-	615	294	9.0	633	296
100	-	604	290	12.4	613	282
150	-	585	272	11.5	601	263
200	-	516	264	11.3	547	255
250	-	286	226	12.6	206	245
300	11.9	193	167	6.4	17	243

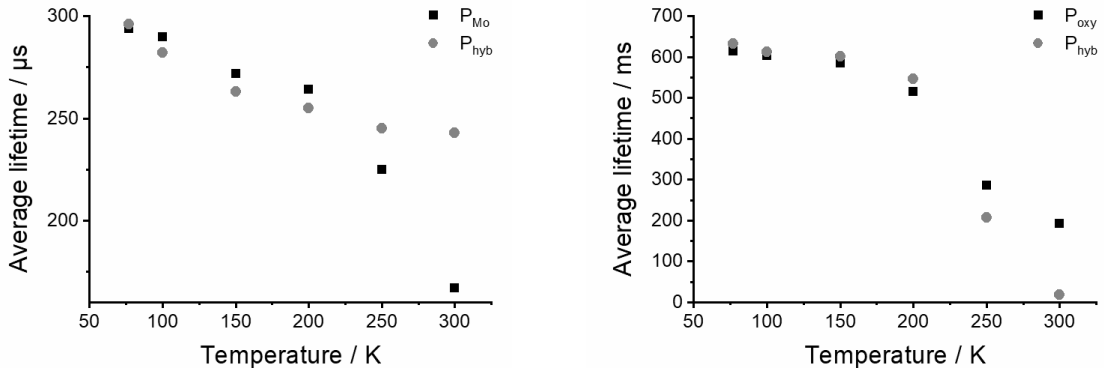

Figure S10. Evolution of the excited state lifetime values of Mo_6 (left) and Oxi (right) with the temperature in P_{Mo}, $P_{hyb,}$ and P_{oxi}.

Brewster technique

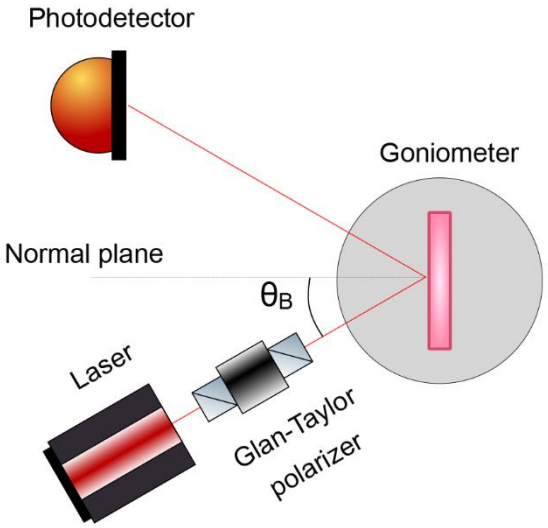

Figure S11. Experimental set-up to measure optical index based on the determination of the Brewster angle for TM polarization.

The following experimental set-up was used to measure the optical index of the P_{hyb} fiber. The measurement is based on the search of the Brewster angle on a flat thin film for the TM polarization. This method[3] enables an accuracy of around 1.10^{-4} on the refractive index measurement compared to usually 4.10^{-6} with the well-known goniometer method based on the minimum deviation by a prism. We can note that this accuracy is largely sufficient since 10^{-2} is only needed to confirm waveguiding properties. In our set-up, a collimated 642 nm laser (Thorlabs LP642-FP200) is polarized thanks to a Glan polarizer enabling to have a TM polarisation with an extinction ratio better than 100000/1. The thin sample under test is positioned on a motorized rotation stage (Newport M-URM80PP). Intensity of the TM reflected light is then measured precisely in the vicinity of the Brewster angle by a Silicium photodiode (Thorlabs SM1PD1A) on a 12 bits oscilloscope (Teledyne Lecroy HDO6104).
Finally, at the Brewster's angle, the angle at which polarized light is not reflected, we determine the refractive index as:

$$\theta_B = \arctan\left(\frac{n_2}{n_1}\right)$$

where n_1 is the air refractive index and n_2 the P_{hyb} refractive index.

FDTD simulations

We performed three-dimensional finite-difference time-domain (FDTD) calculations (Lumerical[6]) to evaluate optical waveguiding of microfiber in the silica fiber. Here, the grid size has been fixed at 10 nm to resolve the curved interface of microfiber. The computational environment is surrounded by perfectly matched layer.
The refractive index of the clad silica (Heraeus F300) has been implemented usin the Sellmeier equation as:

$$n^2(\lambda) = 1 + \frac{B_1\lambda^2}{\lambda^2 - C_1} + \frac{B_2\lambda^2}{\lambda^2 - C_2} + \frac{B_3\lambda^2}{\lambda^2 - C_3},$$

with

B1 = 4.73115591 e-1
B2 = 6.31038719 e-1
B3 = 9.06404498 e-1
C1 = 1.29957170 e-2 μm^2
C2 = 4.12809220 e-3 μm^2
C3 = 9.87685322 e+1 μm^2
The assumptions made were a circular waveguide cross section with a core diameter of 8 µm (based on optical microscope image) and a step refractive index profile as determined with Brewster technique in silica.

Experimental setup for optical propagation measurements

Optical waveguiding of microfibers have been investigated using a home-built setup described in Figure S13. In this setup, the microfiber may be selectively pumped along vertical or longitudinal axis, imaging of the microfiber and spectral analysis of this emission are then performed. In both pumping configuration, emission of the microfiber is first collected by an objective (Nachet x8), then a (50:50) beamsplitter enables us to both image the microfiber and detect the emission. This is realized thanks to a colour camera (Basler acA1920-40uc) and multimode fiber coupling connected to a spectrometer (Ocean Optics Red Tide USB650).
Vertical excitation of microfibers was realized with a laser at 448 nm (Thorlabs LP450-SF15) focalized down to a diameter of around 8 µm through the imaging objective and the dichroic beamsplitter (Thorlabs DMLP90R). In this case, the beamsplitter acts as a pump filter during imaging and spectroscopy analysis.
For longitudinal excitation, the laser beam at 405 nm (Thorlabs S3FC405) is focalized down to a diameter of around 8µm with the same objective (Nachet x8) on the microfiber core. A precise adjustment of the XYZ platform position is then made to maximize coupling between excitation and optical modes supported by our microfiber. Here, the purpose is to realize properly the injection since our microfiber is multimode, thus particular care has been taken to hit core microfiber not the cladding, to avoid excitation of cladding modes.

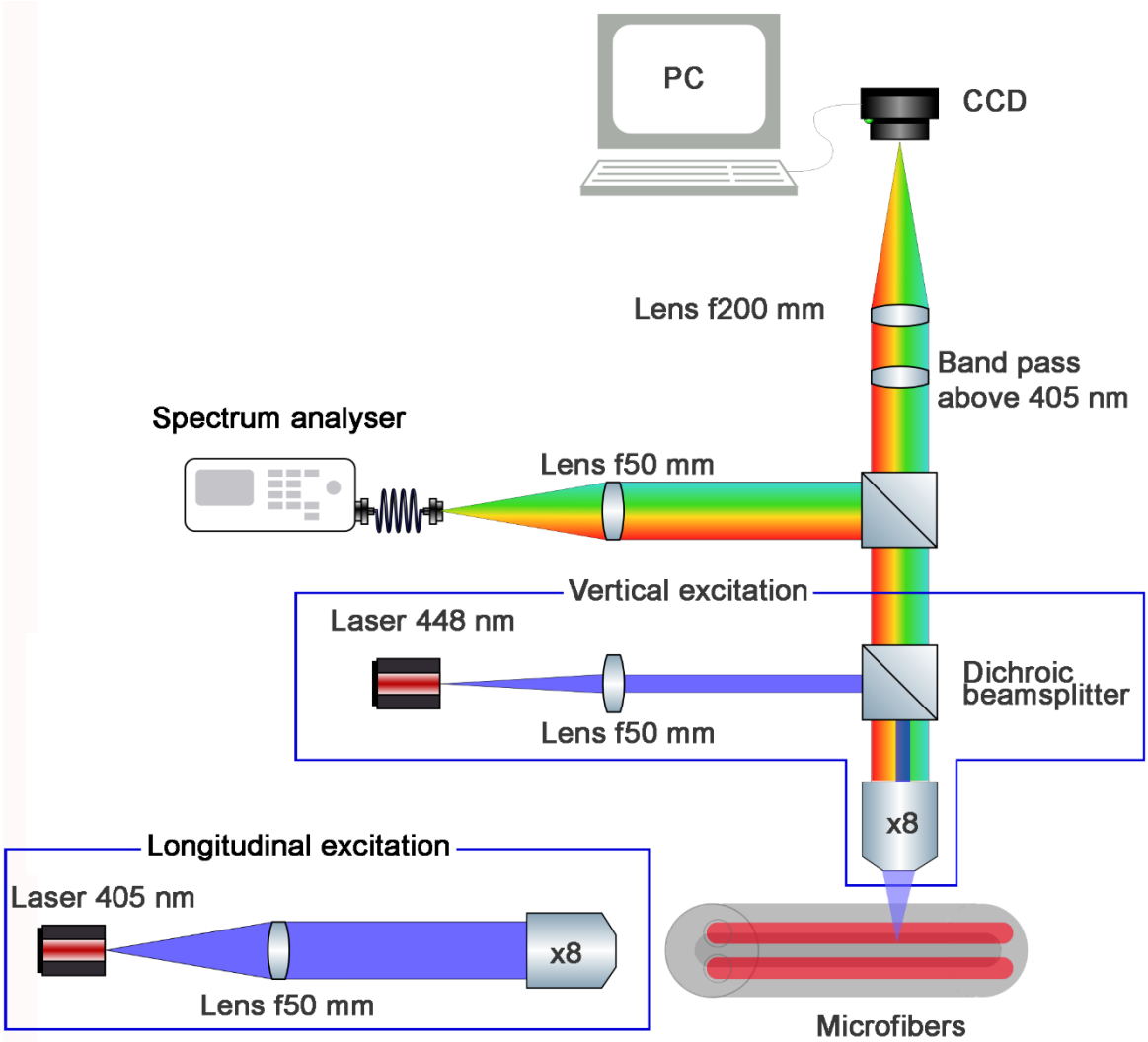

Figure S12. Experimental setup used to investigate photoluminescence waveguiding of microfibers.

CIE coordinates

The CIE chromaticity diagram is used to represent colour as it is perceived by the human eye. Here, CIE colour coordinates were calculated using the open source ColorPy package[4] and reported on the CIE graph.[5] We observed an emission color change from (CIEx=0.49, CIEy=0.38) for thin films to a warm white yellowish emission (CIEx=0.40, CIEy=0.40).

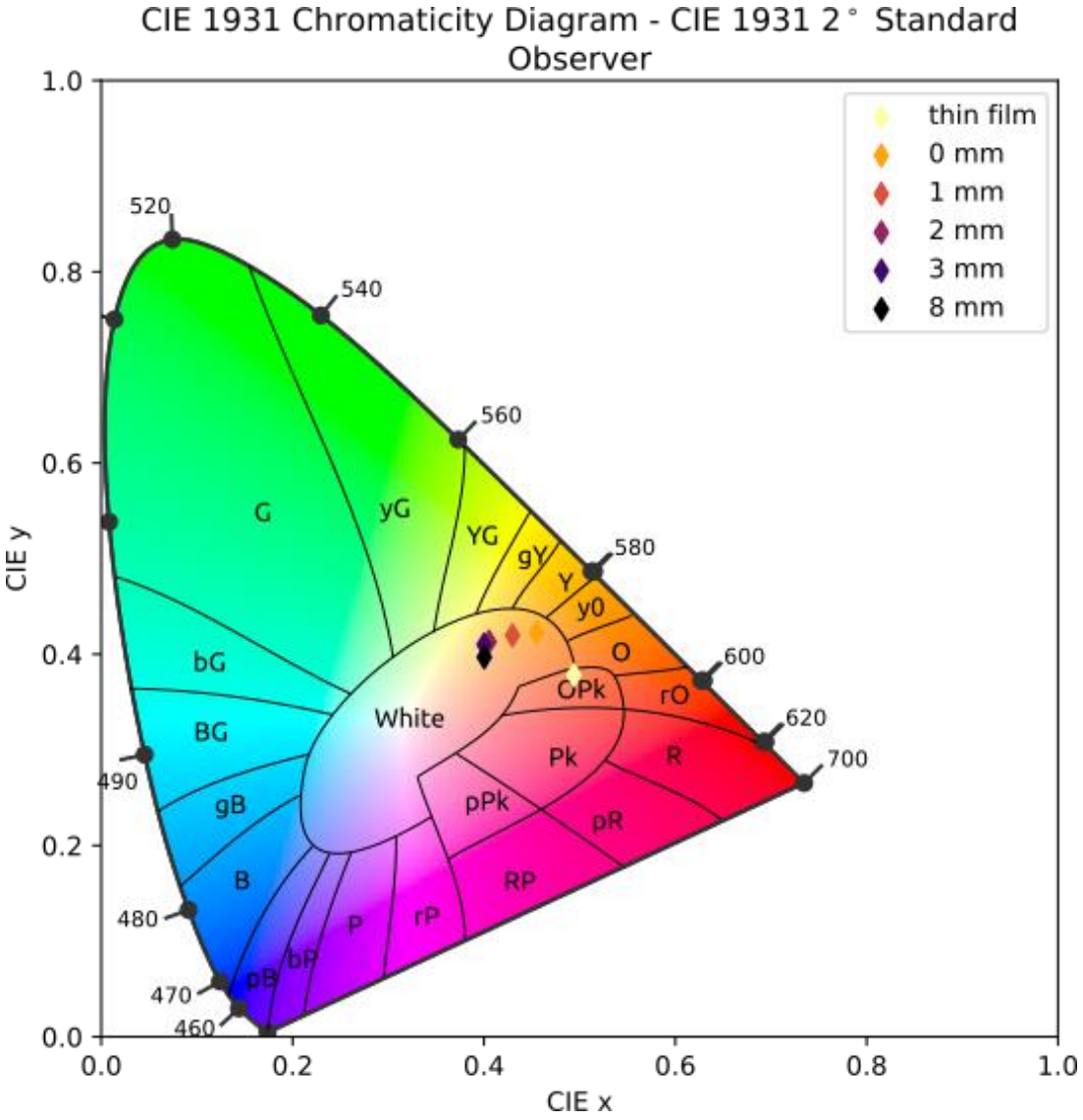

Figure S13. Color rendering along the microfiber in the CIE 1931 Chromacity diagram.

Reference

1. J. R. Lakowicz, *Principles of Fluorescence Spectroscopy, third edition*, Springer, Boston, MA, 2006.
2. P. G. Wu and L. Brand, *Anal. Biochem.*, 1994, **218**, 1-13.
3. C. Bahrim and W.-T. Hsu, *Am. J. Phys.*, 2009, **77**, 337-343.
4. M. Kness, Colorpy - a python package for handling physical descriptions of color and light spectra., http://www.markkness.net/colorpy/ColorPy.html, (accessed 04/23/2021, 2021).
5. S. Gage, D. Evans, M. Hodapp and H. Sorenson, *Optoelectronics Applications Manual*, McGraw-Hill Inc., Blacklick, Ohio, U.S.A. , 1977.
6. L. Inc., https://www.lumerical.com/products/fdtd/, (accessed 04/23/2021).